THE ASTROPHYSICAL JOURNAL, 402:303–310, 1993 January 1

CCD OBSERVATIONS OF THE Hα LINE IN LATE G AND K SUPERGIANTS AND THEIR INTERPRETATION

SUSHMA V. MALLIK
Indian Institute of Astrophysics, Bangalore 560034, India
Received 1991 December 3; accepted 1992 June 30

ABSTRACT

CCD echelle spectra of the Hα line at 6563 Å have been obtained for a sample of 30 G and K supergiants with a spectral resolution of about 0.24 Å. The data clearly indicate that the observed Hα profile is a deep absorption, implying large optical depths in the chromosphere. Also, the line cores are blueshifted in all the stars which suggests the chromospheres are expanding outward. Detailed radiative transfer calculations of Hα have been carried out in a spherically symmetric atmosphere with outward-positive velocity and temperature gradients, including explicitly the effects of ionization. The Hα line profiles have been computed for a wide range of parameters in order to reproduce the observed features of the line. In particular, the role of various dynamical processes has been demonstrated in conjunction with opacity in determining the Hα widths. Reasonably good theoretical fits with the observed profiles yield Hα optical depths in the range 3–20 and outward linear velocity gradients on the order 20 km s^{-1}. Within the framework of our model, the calculations reinforce the idea that the nonthermal velocities have to be as large as 25–30 km s^{-1} to explain the large widths of the observed profiles. The rates of mass outflow have been calculated to lie in the range 10^{-8} to 10^{-9} $M_\odot$ yr^{-1}.

Subject headings: line: formation — stars: chromospheres — stars: late-type — stars: mass loss — supergiants

1. INTRODUCTION

Observations of asymmetric cores of strong metal lines of low excitation in late-type giants and supergiants have confirmed the presence of mass outflows in these stars (Deutsch 1960; Reimers 1977, 1981). The shift of the line core to the blue has been used to determine the terminal velocity reached in the outer layers of these stars (Sanner 1976; Bernat 1977, 1982; Boesgaard & Hagen 1979). It is also evident from several studies in the past that these winds are characterized by large mass fluxes with small speeds and are most likely accelerated in the chromospheres (Goldberg 1979; Stencel & Mullan 1980; Hartmann 1983; Dupree 1986). Although the Ca II H and K lines and the Mg II *h* and *k* lines have been the most extensively used spectral features in chromospheric studies, it is rather difficult to obtain deep exposures at high resolution of these ultraviolet lines in cool stars.

The Hα line at 6563 Å is observed to have a very strong absorption in late-type giants and supergiants (Mallik 1982; Zarro & Rodgers 1984; Cram & Mullan 1985). It is easily accessible and lies in a region of the spectrum where the bulk of the stellar continuum is radiated. From detailed plane-parallel model atmosphere calculations, Cram & Mullan (1985) have shown that the photosphere contributes little to the strength of this line and that most of the absorption forms in the chromosphere. This line is also seen to be asymmetric in the sense that the core is shifted to the blue with respect to the line center, lending further support to the premise that the chromosphere must be expanding. Hα is not an easy line to interpret because of its subordinate nature. Also since the Hα source function is photoionization-dominated, the line does not relate to the specific distribution of density and temperature in the chromosphere. However, Cram & Mullan (1985) have demonstrated that the formation of Hα does depend upon the physical conditions in the chromosphere in a way different from the collision-dominated lines.

The aim of the present study is to investigate the scope of the Hα line as a chromospheric diagnostic in the light of the new CCD spectra of Hα that we have obtained in a sample of G and K supergiants. To interpret these observations, we have performed detailed transfer calculations explicitly including the statistical equilibrium equations for a model H atom with three levels. We have explored several parameters that are crucial to Hα formation in cool supergiants and within the framework of our model have been able to restrict the range of these parameters by comparison with the observed characteristics of the line in our sample. We have tried to show that Hα does provide clues to the optical depths and velocity flows prevailing in the chromospheres. Section 2 contains the observations. Section 3 describes the theoretical framework for the analysis of the line profiles. Implications of the results and conclusions are discussed in § 4.

2. OBSERVATIONS

About 30 late G and K supergiants brighter than $m_v = +7.0$ have been sampled from the Bright Star Catalog (Hoffleit 1982). The Hα spectra of these stars were obtained on a total of 6 nights during 1989 January–March with the coudé echelle spectrograph at the 102 cm Zeiss telescope of the Vainu Bappu Observatory at Kavalur, India using a Thomson CCD detector with the format 384 × 576 pixels, each pixel being 23 μm square in size. A 79 l mm^{-1} echelle grating blazed at 6746 Å in the 34th order where Hα lies and a 300 l mm^{-1} cross disperser grating blazed at 6400 Å in the first order were used in conjunction with a 25 cm camera covering the spectral region between 5700 and 7800 Å. This configuration yielded a dispersion of 7 Å mm^{-1}, or in other words, 0.16 Å $pixel^{-1}$ which with the slit width used for the observations gave a spectral resolution of 0.24 Å. Most of the stars observed are bright and the fluxes of the continuum in the CCD images of these stars are quite high giving S/N ratios of 300 or greater. A good number of bias, comparison (thorium-argon) and flat-field (xenon) frames were taken well spaced out in time each night.

The reduction of the data was carried out with the spectroscopic software package "RESPECT" due to Prabhu & Anupama (1991) where each order of interest in the echelle spectrum can be chosen interactively. The bias and the thermal background are subtracted from the raw spectrum. The pixel-to-pixel sensitivity difference, i.e., the flat-field variation, is also corrected for. The one-dimensional spectrum is then extracted from the two-dimensional image based on the algorithm developed by Horne (1986, 1988). The wavelength calibration of the Hα spectrum was done in two steps. First, the comparison spectrum identified from the atlas of D'Odorico et al. (1984) was used to locate the stellar features in the neighborhood of Hα. Once they were identified, lines of photospheric origin (with lower excitation potential ≥ 2 eV) were chosen to calibrate the stellar spectrum once again. This was done to facilitate the determination of the relative shift of the chromospheric Hα with respect to the photosphere. By measuring the relative shift of the chromospheric Hα with respect to the photosphere, we fix only the gradient, not the zero point of the velocity. The continuum was determined by choosing as many points as possible on the spectrum by visual inspection and then fitting by spline interpolation. Finally, the normalized spectrum was obtained by dividing the observed spectrum by the estimated continuum.

Figure 1 shows the Hα profiles with the adjacent continuum from the reduced spectra of a few representative stars. Two characteristics stand out in these spectra. First, the Hα line is strong with a core as deep as or deeper than 0.2 in all the 30 stars. This implies fairly large optical depths. Also the blow-up profiles in Figure 2 show that they are skewed to the right, i.e., are asymmetric in the sense that the cores are shifted toward blue with respect to the line center. Table 1 gives the list of stars with the measured equivalent widths (EW) in Å and the full widths at half-maximum (FWHM) in Å and km s^{-1}. The EWs lie in the range 1.3–1.8 Å. The FWHMs are between 1.45 and 2.0 Å which translate to velocities in the range 65–100 km s^{-1}. A higher EW is generally accompanied by a larger FWHM. The shift of the line minimum to the blue has been measured for all the stars. These shortward shifts of the core are also listed in Table 1. They lie in the range of -5 to -15 km s^{-1}. The accuracy of the wavelength calibration is 0.05 Å $\equiv$ 2 km s^{-1}. So the positions of the line core minimum have been determined with fairly good accuracy. Velocities are small as found in the earlier studies of the chromosphere.

TABLE 1

OBSERVATIONAL DATA

Star	Sp Type	EW (Å)	FWHM (Å)	FWHM (km s^{-1})	Shift (km s^{-1})
π Pup	K3 Ib	1.61	1.60	73	−6.9
λ Vel	K4 Ib	1.52	1.60	73	−6.4
HR 5089	G9 Ib	1.72	1.96	90	...
HR 6578	K2.5 Ib	1.24	1.56	71	...
HR 2269	K3 Ib	1.28	1.48	68	−4.6
HR 4050	K3 III	1.60	1.76	81	−5.0
HR 3692	K3 Ib	1.45	1.65	75	...
ξ Cyg	K4.5 Ib–II	1.61	1.79	82	−8.7
σ CMa	K7 Iab	1.59	1.56	72	−11.0
ψ Aur	K5 Iab	1.48	1.46	67	...
HR 3612	G7 Ib–II	1.61	1.81	83	...
HR 3225	K3 Ib	1.49	1.69	77	−5.5
HR 2993	K3 Ib	1.44	1.52	70	−5.0
HR 2764	K3 Iab	2.18	2.19	100	−23.3
HR 5742	K4 III	1.54	1.63	75	−18.7
η Per	K3 Ib	1.71	1.85	85	−12.8
ε Gem	G8 Ib	1.70	1.72	79	−14.6
β Pyx	G7 Ib–II	1.42	1.68	77	−4.6
β Ara	K3 Ib–IIa	1.72	1.89	87	−6.4
63 Cyg	K4 Ib	1.62	1.82	83	−7.3
47 Cyg	K2 Ib	1.80	1.88	83	−11.9
41 Gem	K3 Ib	1.45	1.51	69	−13.3
ε Peg	K2 Ib	1.61	1.74	80	−9.6
33 Sgr	K1 Ib	1.55	1.77	81	−5.0
o^1 CMa	K2 Iab	1.53	1.49	68	−5.0
HR 7759	K3.5 IIab	1.47	1.63	75	−5.0
HR 7083	K2 Ib	1.52	1.75	80	−5.0
12 Peg	K0 Ib	2.23	2.85	130	−18.3
ζ Cep	K1 Ib	1.65	1.73	79	−11.9

3. THEORY

To interpret the above characteristics, we treat the radiative transfer problem in spherically symmetric, expanding, non-LTE atmospheres including explicitly the temperature rise of the chromosphere and the effects of ionization of hydrogen. We have suitably modified the comoving frame radiative transfer code of Peraiah (1981) for our purpose. The chromosphere is divided into a number of shells starting from R_*, the stellar radius, up to an R_{max}. Observational evidences (White, Kreidl, & Goldberg 1982; Goldberg et al. 1982; Carpenter et al. 1985) suggest that R_{max} is of the order of a few R_*'s. The chromosphere is described by a velocity distribution $v(r)$, a density distribution $\rho(r)$, a temperature distribution $T(r)$, and a non-thermal velocity parameter ξ_t. A straightforward way to reproduce the observed blue shift of the core is to assume that the velocity is increasing outward. For the sake of simplicity, we adopt a linear velocity gradient. For a mass conservative flow in spherical symmetry, the rate of mass outflow is given by

$$\dot{M} = 4\pi r^2 \rho(r) v(r) . \quad (1)$$

We use $\dot{M}$ as a free parameter. The density distribution is then determined in accordance with the above equation of continuity. $T(r)$ is adopted from the work of Dupree et al. (1984). The adopted temperature profile shows a steep rise from 4000 K at R_* to 8000 K within the first few shells followed by a very slow upward gradient over the rest of the line forming region, with the maximum of 8500 K reaching at R_{max}. Supergiants are known to have low rotation. Therefore we assume in our model that rotation contributes little to the Hα width. Collisional broadening is also negligible owing to the low densities. We assume therefore that Doppler broadening dominates the shape of the Hα line profile. The profile function is of the form

$$\phi(x, \delta) = \frac{1}{\delta\sqrt{\pi}} e^{-x^2/\delta^2} , \quad (2)$$

where

$$x = \frac{\nu - \nu_0}{\Delta\nu_D}$$

and

$$\delta = \frac{\Delta\nu_D(r)}{\Delta\nu_D^{ref}} .$$

$\Delta\nu_D(r)$ is the depth-dependent Doppler width given by

$$\Delta\nu_D(r) = \frac{\nu_0}{c}\sqrt{\frac{2kT(r)}{m} + \xi_t^2} . \quad (3)$$

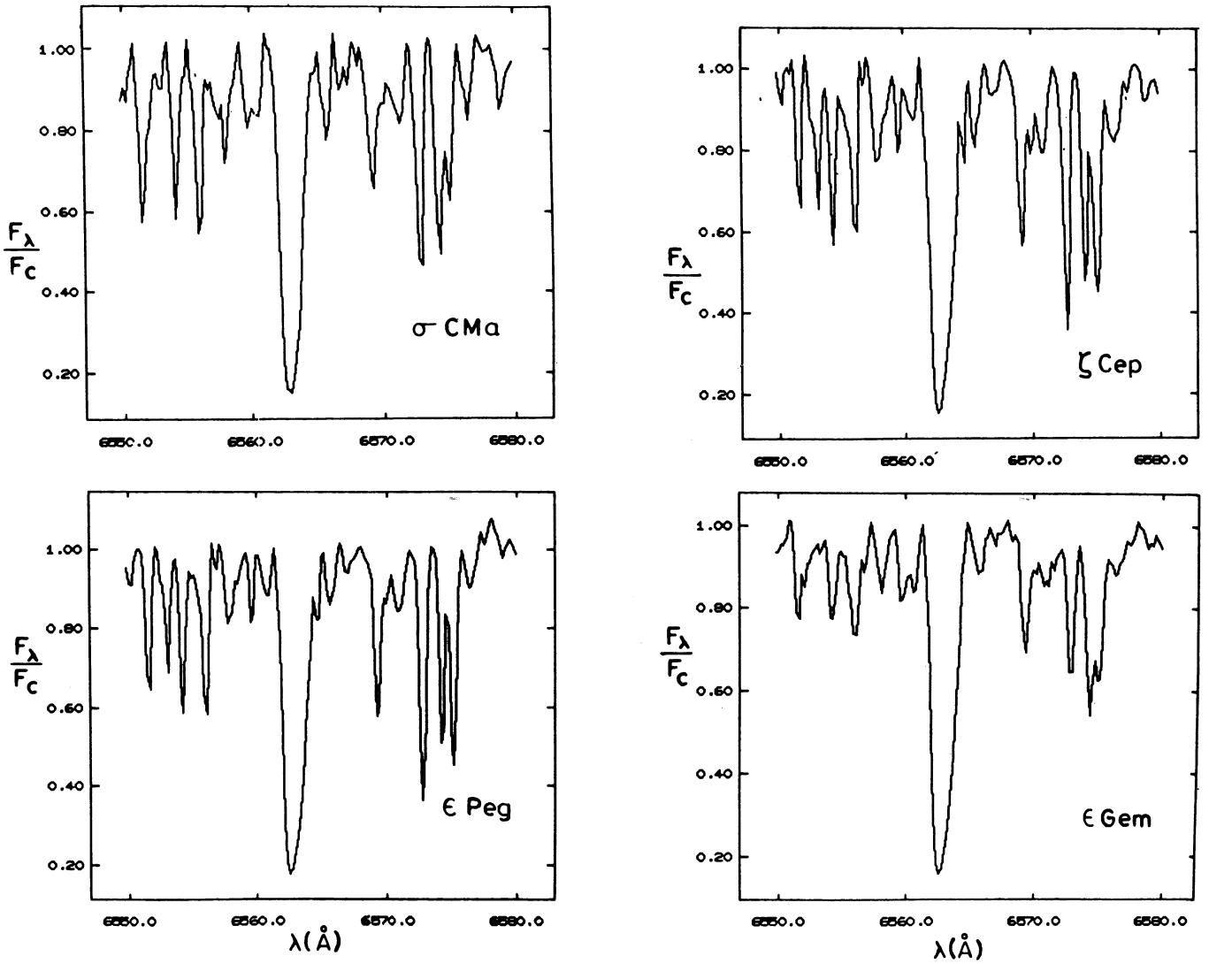

FIG. 1.—CCD spectra of Hα and the adjacent continuum of a few representative stars

$\Delta v_D^{\rm ref}$ refers to the value at $R_{\rm max}$. The underlying photospheric radiation field is introduced as a lower boundary condition represented by a Planck function of radiation temperature $T_R = 4000$ K.

In the earlier calculations (Mallik & Mallik 1988), we assumed that the population in the $n = 2$ level of H is predominantly determined by the balance between photoionizations from level 2 to the continuum and recombinations to that level. This was then used to set up the optical depth scale for Hα in calculating the Hα source function. Also we presupposed that the Hα line source function parametrized for a two-level atom is of the form

$$S_l(r) = (1 - \epsilon) \int \phi_\nu J_\nu d\nu + \epsilon B_\nu , \tag{4}$$

the total source function being equal to

$$S(r) = \frac{\phi(x)}{\beta + \phi(x)} S_l(r) + \frac{\beta}{\beta + \phi(x)} S_c(r) . \tag{5}$$

S_c is the continuum source function assumed to be a Planckian with the depth dependence defined by a dilution factor

$$W(r) = 0.5[1 - (1 - r^{-2})^{1/2}] . \tag{6}$$

ϵ is the collisional deexcitation parameter, and β is the ratio of the continuum to the line opacity. ϵ and β were taken to be depth-independent. The statistical equilibrium equations were not explicitly included in the formalism.

In the present work we have performed calculations including statistical equilibrium equations for the following cases: (1) H atom, levels 2 and 3 plus the continuum; and (2) H atom, levels 1, 2, and 3 plus the continuum. The equations are solved simultaneously with the equation of radiative transfer to obtain self-consistent solutions of the Hα source functions and level populations. An equivalent two-level atom approach as described in Mihalas (1978) is appropriate here. In both the cases, the line source function can be expressed in the form

$$S_l = \gamma \int \phi_\nu J_\nu d\nu + \epsilon B_\nu , \tag{7}$$

where γ and ϵ denote the various collisional and radiative

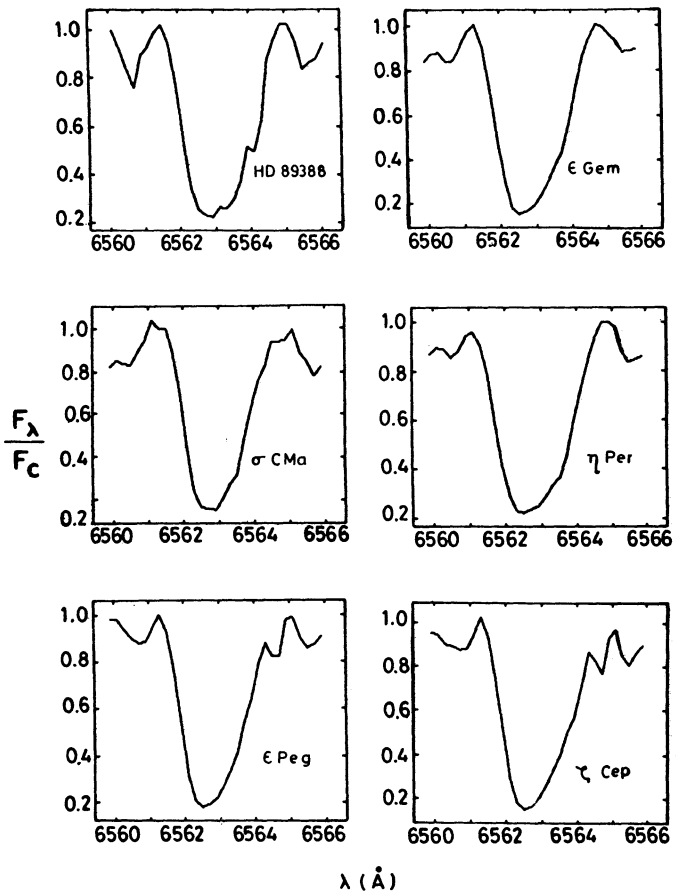

FIG. 2.—Blow-up of the Hα profiles of a few stars

processes that describe the creation and destruction of photons. γ and ϵ are explicitly calculated as a function of the depth.

3.1. *Two-Level Atom Model*

The statistical equilibrium equations give for the population of level 2

$$n_2 = n_p^2 \frac{[\alpha_3(R_{32} + C_{32} + \alpha_2(R_{32} + C_{32} + R_{3c})]}{(R_{23}R_{3c} + C_{23}R_{3c} + R_{2c}R_{32} + R_{2c}C_{32} + R_{2c}R_{3c})} \quad (8)$$

where Rs and Cs denote the radiative and collisional transitions, respectively. We assume that the populations in the levels 1 and 2 are collisionally coupled. Then with the aid of the conservation equation, we obtain n_p through the solution of a quadratic equation.

The Hα source function may be written as

$$S_{23} = \frac{\int \phi_\nu J_\nu d\nu + \epsilon' B_\nu + \theta}{1 + \epsilon' + \eta} \quad (9)$$

where

$$\epsilon' = \frac{C_{32}}{A_{32}}(1 - e^{-h\nu_{32}/kT}),$$

$$\eta = \frac{R_{3c}\alpha_2 - (g_2/g_3)R_{2c}\alpha_3}{A_{32}(\alpha_2 + \alpha_3)},$$

$$\theta = \frac{2h\nu^3}{c^2}\frac{g_2}{g_3}\frac{R_{2c}\alpha_3}{A_{32}(\alpha_2 + \alpha_3)}.$$

3.2. *Three-Level Atom Model*

In this case, the statistical equilibrium equations for the levels 1, 2, and 3 are simultaneously solved along with the conservation equation to obtain n_1, n_2, n_3, and n_p in terms of the departure coefficients b's, their ratios, and the total hydrogen density n_H. n_2 in particular is of the form

$$n_2 = \frac{n_H}{[1 + (b_2/b_1)(n_2/n_1)^* + (b_3/b_1)(n_3/n_1)^* + (1/b_1)(n_p/n_1)^*]}, \quad (10)$$

where $n_i = n_i^*(b_i/b_i^*)$. Radiative detailed balance is assumed in Lyman lines and the Lyman continuum.

The Hα source function is once more of the form

$$S_{23} = \frac{\int \phi_\nu J_\nu d\nu + (\epsilon' + \theta)B_\nu(T)}{1 + \epsilon' + \eta}, \quad (11)$$

where

$$\epsilon' = \frac{C_{32}}{A_{32}}(1 - e^{-h\nu_{32}/kT}),$$

$$\eta = \frac{R_{3c}(n_p^2\alpha_2 + n_1C_{12} - n_2C_{21}) - (g_2/g_3)R_{2c}(n_p^2\alpha_3 + n_1C_{13} - n_3C_{31})}{A_{32}(n_p^2\alpha_2 + n_p^2\alpha_3)},$$

$$\theta = (1 - e^{-h\nu_{23}/kT})\frac{n_2^*}{n_3^*}\frac{R_{2c}(n_p^2 + n_1C_{13} - n_3C_{31})}{A_{32}(n_p^2\alpha_2 + n_p^2\alpha_3)}.$$

As is apparent from these expressions, the populations require an a priori knowledge of the radiation field and the latter in turn depends upon the populations. The solution is obtained iteratively where an initial guess of the populations is made to calculate the Hα source function and the radiation fields R_{23} and R_{32} which are then used to calculate the b ratios, b's, and the new populations. The radiation fields are then recomputed and used to recalculate new populations. The process is carried until convergence is achieved in both the radiation field and populations. About five to six iterations were adequate to achieve convergence. Before obtaining the final solutions, we checked our program for flux conservation in the pure scattering case. With the converged n_2 solutions, Hα optical depth scales were set up. In order to fit the observed characteristics of the Hα line, theoretical line profiles were computed for both the two-level and the three-level atom models for mass-loss rate $\dot{M}$ in the range 10^{-9} to 10^{-8} $M_\odot$ yr^{-1}, V_{max} = 5–25 km s^{-1}, $R_{max} = 2R_*$ and $5R_*$, and ξ_t = 20–40 km s^{-1}.

4. RESULTS AND CONCLUSIONS

The sensitivity of the profiles to the various parameters has been explored and the following trends have been observed for both the models.

1. For a given $\dot{M}$, the computed line profiles are extremely sensitive to V_{max}; the higher the V_{max}, the shallower is the profile in conformity with the equation of continuity as shown in Figure 3*a*. For a given R_{max}, for various combinations of $\dot{M}$ and V_{max} that result in the same optical depth, the corresponding profiles have roughly the same EW and the same depth in the core. Thus it is the optical depth that uniquely determines the shape and the strength of the Hα profile.

2. For the same M and V_{max}, the profiles are much deeper for a higher R_{max} (Fig. 3*b*). This is not entirely an optical depth

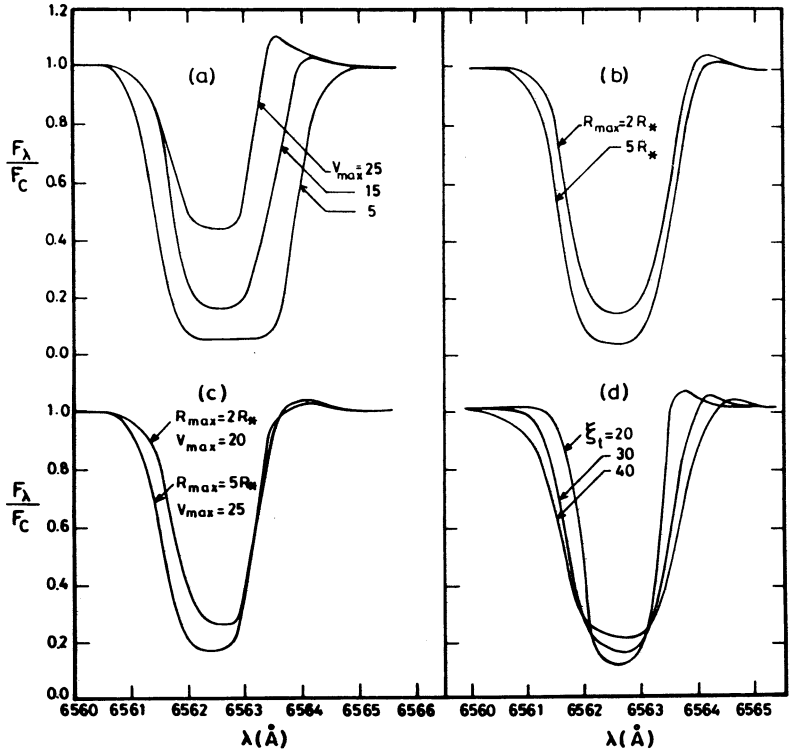

FIG. 3.—Computed profiles for a three-level atom model with $\dot{M} = 5 \times 10^{-9}\ M_\odot\ \mathrm{yr}^{-1}$. (*a*) $R_{max} = 2R_*$, $\xi_t = 30\ \mathrm{km\ s}^{-1}$. (*b*) $V_{max} = 15\ \mathrm{km\ s}^{-1}$, $\xi_t = 30\ \mathrm{km\ s}^{-1}$. (*c*) $\tau = 3.1$, $\xi_t = 30\ \mathrm{km\ s}^{-1}$. (*d*) $R_{max} = 2R_*$, $V_{max} = 15\ \mathrm{km\ s}^{-1}$.

effect as is evident from a comparison of two profiles with similar optical depths but different R_{max}'s (Fig. 3*c*). The larger extent produces a stronger absorption. As a result a lower $\dot{M}$ and a lower n_H are required with a higher R_{max} to produce a reasonable fit with observations.

3. The computed profiles become successively deeper for lower turbulence parameter ξ_t for a given choice of $\dot{M}$ and V_{max} as displayed in Figure 3*d*. Even though the optical depth is higher, EW is lower because of the lower Doppler width. So a higher $\dot{M}$ is required to fit the observed profile when a lower ξ_t is used.

Figure 4 shows the observed profiles for six stars with the superposed theoretical profiles. For a better fit, one or more parameters could be tuned in more finely. However, the emphasis has been on matching the gross characteristics like the FWHM, the depth, the EW, and the blue asymmetry of the line core. In particular, the observed profile of ϵ Gem has a good fit in the case of the three level atom model with $R_{max} = 2R_*$, $\dot{M} = 7 \times 10^{-9}\ M_\odot\ \mathrm{yr}^{-1}$, $V_{max} = 20\ \mathrm{km\ s}^{-1}$, and $\xi_t = 30\ \mathrm{km\ s}^{-1}$. With a higher ξ_t of 40 km s^{-1}, a lower $\dot{M}$ of 5×10^{-9} $M_\odot\ \mathrm{yr}^{-1}$ fits the observed shape better. Also with $R_{max} = 5R_*$, $\dot{M} = 4 \times 10^{-9}\ M_\odot\ \mathrm{yr}^{-1}$ fits the observed profile quite well.

All the computed profiles have a small red emission to the right of the absorption lying above the continuum. This is a consequence of the model chosen. With a spherically symmetric, radially and slowly accelerating envelope of the extent of the order of the stellar radius surrounding the star, the material in front of the stellar disk gives rise to the absorption and the material in the envelope to the sides of the disk gives a small emission. In reality, small emission components have also been detected in some of our program stars lying either to the right or to the left of the strong Hα absorption, thus indicating both upflows and downflows. Similar observations have been reported by several authors in the past (Cohen 1976; Mallia & Pagel 1978; Cacciari & Freeman 1981). Since we have not incorporated complicated velocity flows in our model, the present study has only tried to simulate the absorption profile of Hα and uses it to probe the physical conditions of the accelerating layers of the cool chromospheres.

The chromospheric optical depths, the total hydrogen densities at R_* and the expansion velocities at R_{max} obtained from our analysis are displayed in Table 2 and Table 3 for 22 stars for each of the two models for a given set of parameters. We conclude the following:

1. The total hydrogen densities at R_* and the optical depths in the chromosphere that match the observed equivalent widths are respectively in the range of $n_H(R_*) = 1 \times 10^9$–$3.6 \times 10^9\ \mathrm{cm}^{-3}$ and $\tau_{H\alpha} = 3$–20. For the model atom with three levels, the densities and the optical depths are lower than for the case with two levels. Also the present values are much lower (almost by an order of magnitude) than those obtained from our earlier transfer calculations. The rates of mass outflow that fit the observed characteristics of Hα lie in the range of 2×10^{-9} to $1.4 \times 10^{-8}\ M_\odot\ \mathrm{yr}^{-1}$ and are listed in Tables 2 and 3. These are much lower than the previously estimated values (Mallik & Mallik 1988) which were in the range of 10^{-7} to $10^{-8}\ M_\odot\ \mathrm{yr}^{-1}$. Few specific estimates exist for mass-loss in G and K supergiants. Certainly none exist with Hα as the diagnostic. Instead, the blue-displaced absorption components in the Mg II and Ca II resonance lines have been exploited much more to determine the outflow velocities and mass-loss rates. Reimers (1975) obtained $\dot{M}$ in the range of 10^{-8} to $2 \times 10^{-7}\ M_\odot\ \mathrm{yr}^{-1}$ for several G and K Ib supergiants determined by circumstellar line modeling. According to

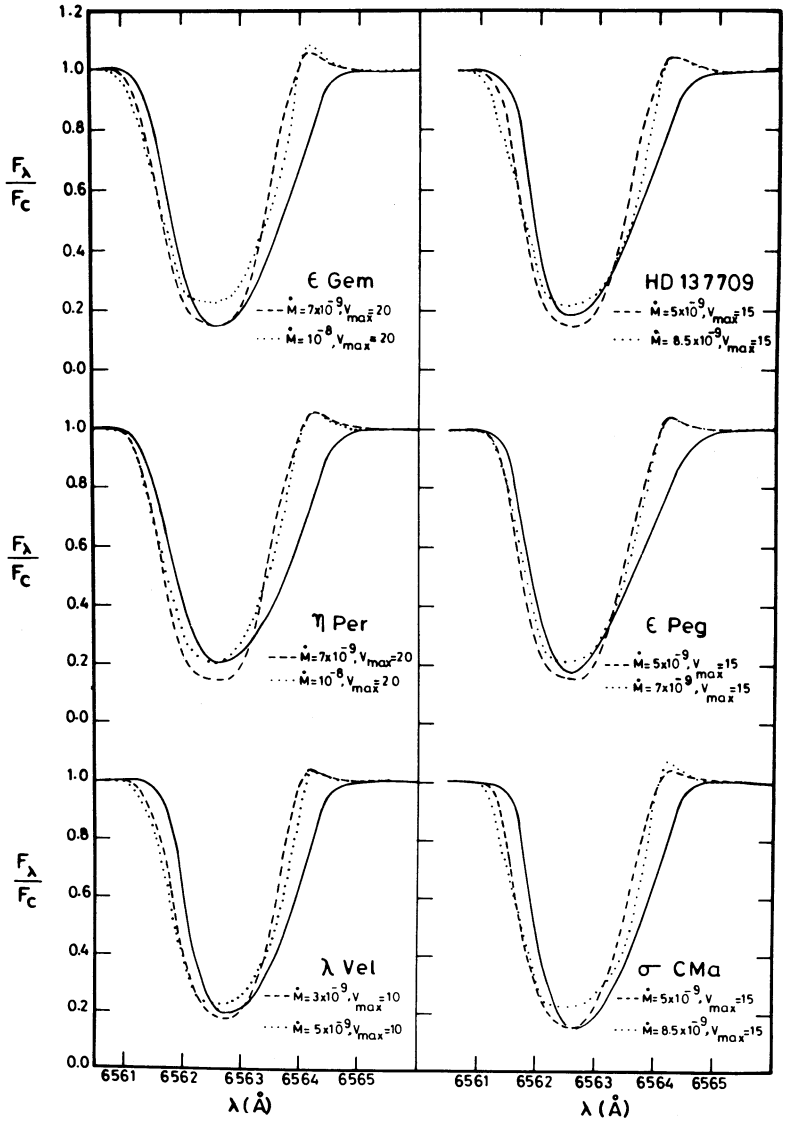

FIG. 4.—Superposition of the computed profiles over the observed Hα profile. The solid line denotes the observed line profile; the dotted line, computed profile for a three-level atom model; the dashed line, the computed profile for a two level atom model. $R_{max} = 2R_*$ and $\xi_t = 30$ km s^{-1}.

Drake (1986), radio continuum techniques provide the most reliable method of estimating $\dot{M}$ for these stars. From radio continuum measurements, Drake & Linsky (1985) inferred upper limits to $\dot{M} \approx 2 \times 10^{-9}\ M_\odot\ \mathrm{yr}^{-1}$ for G and K supergiants, which is much lower than Reimers's results. The discrepancy is primarily attributed to the uncertainties in the ionization level of the winds. The mass outflow estimates obtained in the present study are lower than those estimated by Reimers and are quite close to the radio results.

Since there is only a marginal difference in the results of the three-level atom model from those of the two-level atom, our conclusions may not change by increasing the number of levels further. Since the photoionization edges for levels 2 and 3 lie very close to where the bulk of the radiation in these stars is, the processes we have considered are the most predominant ones and control the n_2 population. We therefore believe that a three-level atom model adequately describes the Hα formation. However, it would be important to see how a relaxation of the assumption of radiative detailed balance in the Lyman continuum and Lyman lines affects the n_2 population and hence the Hα optical depth. We had treated this problem separately by considering levels 1 and 2 and the continuum and solved for transfer in the Lyman-continuum including explicitly the effects of Lyα escape (Mallik, Mallik, & Rao 1991). Our calculations showed that there was a drastic decrease in the hydrogen ionization and a highly overpopulated n_1 resulted with only a moderately increased n_2 relative to the case of radiative detailed balance. Luttermoser & Johnson (1992) in their model atmosphere calculations of red giant stars have also obtained similar results when the condition of radiative detailed balance is relaxed. The current calculations already indicate a much higher n_2, and we hope a further moderate increase due to the relaxation of the condition of radiative detailed balance will change the result only marginally.

2. Apart from opacity effects, it is also worth exploring the extent to which various dynamical processes govern the behavior of the Hα line profile. Because of the temperature rise in the chromosphere, the thermal broadening term in the profile function is not negligible; it varies from ~ 8 to ~ 12 km s^{-1} across the chromosphere. But it is far from enough to match

TABLE 2

CHROMOSPHERIC DENSITIES, OPTICAL DEPTHS, VELOCITIES, AND MASS OUTFLOW RATES: TWO-LEVEL ATOM MODEL: $R_{max} = 2R_*$, $\xi_t = 30$ km s^{-1}

Star	$n_H(R_*)$ (10^9 cm^{-3})	V_{max} (km s^{-1})	τ	$\dot{M}/M_\odot$ (10^{-9} yr^{-1})
π Pup	1.9	12.5	6.8	5.5
λ Vel	1.7	12.0	5.3	4.85
HR 2269	1.8	9.0	5.7	3.7
HR 4050	2.4	9.5	10.2	5.4
ξ Cyg	2.4	14.0	9.3	7.9
σ CMa	1.9	17.75	6.1	7.7
HR 3225	1.9	10.4	6.1	4.65
HR 2993	2.0	9.5	7.6	4.4
HR 5742	1.8	30.0	7.1	12.3
η Per	2.4	21.75	9.4	11.95
ϵ Gem	2.7	23.0	11.2	14.5
β Pyx	2.0	9.0	9.3	4.3
β Ara	3.6	11.0	20.0	9.2
63 Cyg	1.8	13.0	7.5	5.6
47 Cyg	2.9	20.0	12.5	13.4
41 Gem	1.7	22.5	4.7	8.75
ϵ Peg	2.2	15.25	7.8	7.9
33 Sgr	2.3	9.5	8.9	5.0
o^1 CMa	2.2	9.5	8.7	4.9
HR 7759	2.1	9.5	8.0	4.55
HR 7083	2.2	9.5	8.6	4.85
ζ Cep	2.4	20.0	8.9	11.1

TABLE 3

CHROMOSPHERIC DENSITIES, OPTICAL DEPTHS, VELOCITIES, AND MASS OUTFLOW RATES: THREE-LEVEL ATOM MODEL: $R_{max} = 2R_*$, $\xi_t = 30$ km s^{-1}

Star	$n_H(R_*)$ (10^9 cm^{-3})	V_{max} (km s^{-1})	τ	$\dot{M}/M_\odot$ (10^{-9} yr^{-1})
π Pup	1.6	11.75	6.7	4.35
λ Vel	1.4	11.25	5.8	3.80
HR 2269	1.4	8.5	3.8	2.8
HR 4050	1.7	9.0	5.9	3.6
ξ Cyg	1.5	14.3	5.9	5.0
σ CMa	1.5	17.5	6.3	6.1
HR 3225	1.4	10.0	5.1	3.3
HR 2993	1.5	9.25	4.6	3.15
HR 5742	1.4	25.0	5.4	8.45
η Per	1.7	20.7	7.2	8.0
ϵ Gem	1.6	23.75	6.8	9.1
β Pyx	1.6	8.5	4.5	3.1
β Ara	1.7	11.25	7.7	4.45
63 Cyg	1.6	12.5	6.6	4.55
47 Cyg	1.8	19.5	8.1	8.3
41 Gem	1.4	21.75	4.8	6.9
ϵ Peg	1.5	15.5	6.2	5.5
33 Sgr	1.6	9.0	7.5	3.45
o^1 CMa	1.6	9.0	7.4	3.4
HR 7759	1.5	9.25	7.3	3.2
HR 7083	1.6	9.25	7.9	3.4
ζ Cep	1.6	20.0	6.1	7.35

the observed width. Velocity gradients giving rise to the asymmetric shape of the profile also increase the width; every 10 km s^{-1} increase in V_{max} increases the FWHM by 2–4 km s^{-1}. Since the observed core displacements restrict V_{max} to 20 km s^{-1} or less, as the present models show, the outward expansion does not explain the large widths either. As pointed out earlier, there is a linear correlation between the EW and the FWHM, implying a microturbulent origin of the widths rather than a macroturbulent one. We used the ξ_t term in the profile function as a free parameter and several runs with different values suggested that ξ_t as large as 25–30 km s^{-1} is needed to explain the widths. A higher optical depth makes the profiles wider but also much deeper, and still not wide enough to match the observed widths for a given EW. Increasing the number of levels also makes the line slightly deeper, not wider. Our calculations have thus reinforced the idea that for a simultaneous good fit of the width, EW, and asymmetry, nonthermal fields as large as 25–30 km s^{-1} are required.

There are some indications that turbulence increases with height in the chromospheres of giants and supergiants (Fosbury 1973). Hartmann & Avrett (1984) in their chromospheric model of α Ori used a variable turbulent parameter with a value of 3 km s^{-1} at the base of the chromosphere to 11 km s^{-1} at about $2R_*$, declining to 4 km s^{-1} at $6R_*$. Their results, however, indicated that the turbulent velocities used in the model were too low, and better fits could be obtained if the values were increased by a factor of 2. A detailed information of the depth dependence of various physical parameters across the chromosphere could be derived from the study of eclipses in the ζ Aur systems (Che, Hempe, & Reimers 1983; Reimers & Schroder 1983; Che & Reimers 1983; Griffin et al. 1990). These systems consist of a K supergiant and a main-sequence B star. As the B star goes behind the K supergiant, its bright ultraviolet radiation seen through the chromosphere of the K supergiant at different depths gives clues to the variation of the physical conditions across the chromosphere. Extensive *IUE* observations of ζ Aur systems at different phases of the secondary eclipse have indicated that nonthermal velocities in the primary K supergiant chromosphere increase with height (Schröder 1985). Such studies in future should further aid the understanding of the physical phenomena in the outer atmospheres of cool stars.

I thank D. C. V. Mallik for several helpful comments and for a critical reading of the manuscript. I have also benefited from discussions with D. Mohan Rao. Special acknowledgement is due to A. K. Pati for his invaluable help during observations with the CCD detector. I am also indebted to T. P. Prabhu for assistance with the software package for the data reduction. Last, I am especially grateful to the two anonymous referees for very important suggestions which helped improve the paper considerably.

REFERENCES

Bernat, A. P. 1977, ApJ, 213, 756
———. 1982, ApJ, 252, 644
Boesgaard, A. M., & Hagen, W. 1979, ApJ, 231, 128
Cacciari, C., & Freeman, K. C. 1983, ApJ, 268, 185
Carpenter, K. G., Brown, A., & Stencel, R. E. 1985, ApJ, 289, 676
Che, A., Hempe, K., & Reimers, D. 1983, A&A, 126, 225
Che, A., & Reimers, D. 1983, A&A, 127, 227
Cohen, J. 1976, ApJ, 203, L127
Cram, L. E., & Mullan, D. J. 1985, ApJ, 294, 626
Deutsch, A. J. 1960, in Stars and Stellar Systems, 6, Stellar Atmospheres, ed. J. L. Greenstein (Chicago: Univ. of Chicago Press), 543
D'Odorico, S., et al. 1984, Scientific Report, No. 2 (European Southern Observatory)
Drake, S. A. 1986, in Fourth Cambridge Workshop on Cool Stars, Stellar Systems and the Sun, ed. M. Zeilik & D. M. Gibson (Berlin: Springer-Verlag), 369
Drake, S. A., & Linsky, J. L. 1986, AJ, 91, 602
Dupree, A. K. 1986, ARA&A, 24, 377
Dupree, A. K., Avrett, E. H., Hartmann, L., & Smith, G. 1984, in Proc. 4th European IUE Conf. (Noordwijk: European Space Agency SP-218), 191
Fosbury, R. A. E. 1973, A&A, 27, 129
Goldberg, L. 1979, QJRAS, 20, 361

Goldberg, L., et al. 1982, in Second Cambridge Workshop on Cool Stars, Stellar Systems and the Sun, ed. M. S. Giampapa & L. Golub (SAO Spec. Rept. 392), 131
Griffin, R. E. N., Griffin, R. F., Schröder, K. P., & Reimers, D. 1990, A&A, 234, 284
Hartmann, L. 1983, Highlights Astron., 6, 549
Hartmann, L., & Avrett, E. H. 1984, ApJ, 284, 238
Hoffleit, D. 1982, Bright Star Catalog (4th ed.; New Haven: Yale Univ. Observatory)
Horne, K. 1986, PASP, 98, 609
———. 1988, in New Directions in Spectrophotometry, ed. A. G. D. Philip, D. Hayes, & S. Adelman (Schenectady: L. Davis), 285
Luttermoser, D. G., & Johnson, H. R. 1992, ApJ, 388, 579
Mallia, E. A., & Pagel, B. E. J. 1978, MNRAS, 184, 55
Mallik, S. V. 1982, J. Astrophys. Astron., 3, 39
Mallik, S. V., & Mallik, D. C. V. 1988, MNRAS, 233, 649
Mallik, S. V., Mallik, D. C. V., & Rao, D. M. 1991, A&A, 243, 463
Mihalas, D. 1978, Stellar Atmospheres (2d ed.; San Francisco: Freeman)
Peraiah, A. 1981, Ap&SS, 77, 243
Prabhu, T. P., & Anupama, G. C. 1991, Bull. Astr. Soc. India, 19, 97
Reimers, D. 1975, in Problems in Stellar Atmospheres and Envelopes, ed. B. Baschek, W. H. Kegel, & G. Traving (Berlin: Springer-Verlag), 229
———. 1977, A&A, 57, 395
———. 1981, in Physical Processes in Red Giants, ed. I. Iben, Jr. & A. Renzini (Dordrecht: Reidel), 269
Reimers, D., & Schröder, K. P. 1983, A&A, 124, 241
Sanner, F. 1976, ApJS, 32, 115
Schröder, K.-P. 1985, A&A, 147, 103
Stencel, R. E., & Mullan, D. J. 1980, ApJ, 238, 221
White, N. M., Keidl, T. J., & Goldberg, L. 1982, ApJ, 254, 670
Zarro, D. M., & Rodgers, A. W. 1983, ApJS, 53, 815